Journal of Fusion Energy (2023) 42:30
https://doi.org/10.1007/s10894-023-00367-7

ORIGINAL RESEARCH

Fundamental Scaling of Adiabatic Compression of Field Reversed Configuration Thermonuclear Fusion Plasmas

D. Kirtley[1] · R. Milroy[1]

Accepted: 22 June 2023 / Published online: 13 July 2023

Abstract
Field Reversed Configuration (FRC) plasmas are plasma devices that have demonstrated that through magnetic compression they can be heated to thermonuclear fusion conditions in the parameter space of an energy-producing generator Kirtley et al. (IEEE Symposium on Fusion Engineering, 2021). Of particular interest, FRCs are high-beta, in that the plasma particle kinetic energy is in balance with an externally applied magnetic field at all stages of operation. The following work will show that a cylindrical approximation for the energy and particle distribution within an FRC can, within 11%, match the fusion performance results of both full Magnetohydrodynamic (MHD) simulations as well as all robust, modern theoretical spatial and energy distribution models. Further, by using the simplified cylindrical model, detailed fusion reaction, radiation, and energy transport equations are now numerically-tractable and can be modelled over a wide parameter space. In the second section of this work, a detailed numerical model will be presented with the key theoretical performance of the compression of high-beta fusion plasmas in both deuterium–tritium (D–T) and deuterium–helium-3 (D–He-3) fuels. As will be shown, a high-beta D–He-3 plasma outperforms a low-beta D–T fuel and can theoretically yield a net-positive fusion generator.

Keywords Field reversed configuration · FRC · Thermonuclear fusion · Helion · Helium-3 · LHD

Introduction

Field Reversed Configuration (FRC) plasmas are self-organized, closed-field plasma configurations created in an open-ended, cylindrical magnetic topology. They have been explored in a range of experimental programs dating to the 1980s and recently have shown to have the ability to be compressed and heated to well over 1 keV electron and 8 keV ion temperatures [2, 3]. Detailed FRC reactor designs have been completed for steady operating systems in a variety of fuels, including D–He-3 [4, 5]. And while theoretically Magnetohydrodynamic (MHD)-unstable to tilt, FRCs have demonstrated kinetic stabilization of the tilt mode to many Alfvén times [6, 7]. Further, particle transport in FRCs, as expected, vastly exceed traditional theta pinch topologies and have been represented as a modified Lower Hybrid Drift (LHD) diffusion [8–10]. Helion Energy is pursuing the production and commercialization of FRC fusion generators that supersonically merge two high-flux FRCs and then compress them to thermonuclear conditions. Of particular interest, as FRCs are high-beta, they may be suitable for operation in both advanced, low-neutron fusion fuels as well as enable direct, inductive electricity extraction. In the following paper, the fundamental scaling of a pulsed D–He-3 generator using an FRC plasma configuration will be described. In the first section, stability and radial distributions of species temperature and density will be explored. Theoretical, experimental, and computational models will be compared and the total fusion power accuracy of several simplified models will be detailed. Using these simplifications, the following section details a fundamental scaling approach which compares relevant fusion power loss and gain phenomena. Finally, a detailed comparison of fusion fuels and generator operating regime is given prior to notes on commercializing the outlined technology.

✉ D. Kirtley
dkirtley@helionenergy.com

[1] Helion Energy, Inc., Everett, WA, USA

Particle Distributions in Field Reversed Configuration Plasmas

Field Reversed Configurations obey several well-proven approximations. First among these is that, unlike most fusion plasmas, within the high-beta FRC (where the separatrix radius is large), the ion and electron temperatures are spatially uniform, but not equal, which has been shown experimentally and confirmed theoretically and computationally. Further, ion and electron densities can be represented by a rigid rotor profile within the separatrix and a small range of edge profile assumptions. In the following sections, these will be shown, then wholistic performance parameters will be given based on these approximations and compared with a complete 2D MHD computational model and relevant theoretical distribution models.

Stability

FRC stability has been explored in detail and will be given a cursory review. In full MHD, fluid treatment, a high-beta, cylindrical plasma, such as the FRC, is MHD unstable to the internal tilt instability in a few Alfven times. However, the earliest experimental programs showed that, provided sufficient elongation, FRCs can be formed and compressed without any tilt concerns [41]. Fundamentally, FRC tilt stability depends on the kinetic nature of the plasma, and this kinetic nature is often characterized by the parameter s which is a measure of the number of internal ion gyro radii that separates the radial field null R and the separatrix r_s. This parameter is defined as:

$$s = \int_R^{r_s} \frac{rdr}{r_s \rho_i} \tag{1}$$

where ρ_i is the ion gyro radius at the FRC separatrix. Provided the s/ε, where ε is the elongation, is less than 3, FRCs do not undergo tilt. FRCs are also subject to wobble and rotational instabilities. Both are believed to occur due to preferential particle orbit losses which have been shown can be stabilized through end biasing [19] and neutral beam injection, and are on the timescale of the particle confinement time. For a pulsed system, this removes operational constraints. It is an a priori assumption that any practical FRC design would have the fundamental tilt scaling as a design requirement. As there are no internal magnetic islands or strong thermal gradients, it is not expected, nor observed, that any ion turbulence or ion shear-driven instabilities will occur in FRCs, unlike other magnetic configurations. Tearing mode instabilities have been investigated in depth in FRCs. In general, it is believed that there is continuous minor tearing and relaxation going on within the edge profile of an FRC, that leads to a tearing-stable profile with some increased diffusion rates, but no bulk instability behavior [11]. No other instabilities have yet been observed in FRC plasmas, now operating well into the thermonuclear plasma regime.

Ion Temperature

As described above, the s parameter for a stable FRC is in the range of 1 to 3, almost ensuring a uniform T_i profile within the FRC. It is important to note that ion temperature within the FRC can be temporally different, different by species, and/or follow non-Maxwellian distributions; however, those temperatures are spatially uniform. This is well-characterized in FRC simulation and experimentation. In a Helion FRC, ion temperature is constant (within 5%).

Figure 1 shows a Cygnus simulation of the radial cross section of a low temperature FRC, showing ion temperature and gyro radius. Cygnus is a 2-D axisymmetric Hall-MHD code that is capable of modeling FRC formation, translation, merging, and compression. The Cygnus code was developed by D. C. Barnes for general FRC modeling applications, and the code was improved considerably as part of Helion's ARPA-E program, "Staged Magnetic Compression of FRC Targets," and validated experimentally on Helion's 5th fusion prototype [12]. The current version of the code includes support for arbitrary axisymmetric geometries using a cut-cell formulation on a finite difference discretization, allows for static and dynamic external circuits to be coupled to the MHD equations, and uses a semi-implicit time advance in the code to mitigate numerical instabilities and prohibitive Courant–Friedrichs–Lewy (CFL) time step limitations. For this simulation, there is an average of 2.5 ion gyro radii from the center to the edge of the plasma, and less than one ion gyro radius between the field null and separatrix. Figure 2 shows a simulation for the axial and radial distribution of ion temperature as well as the separatrix radius, r_s, coil radius,

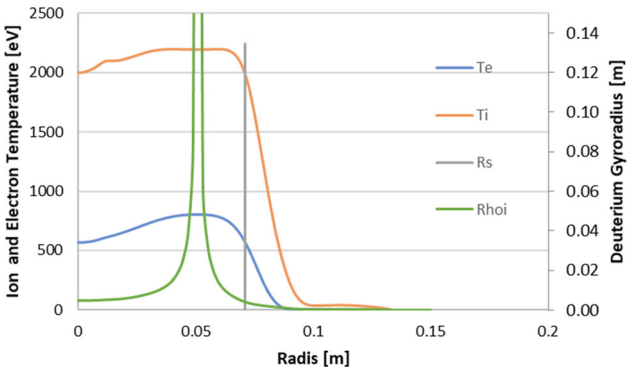

Fig. 1 Radial profiles for ion and electron temperature, separatrix radius r_s and ion gyro radii ρ_i

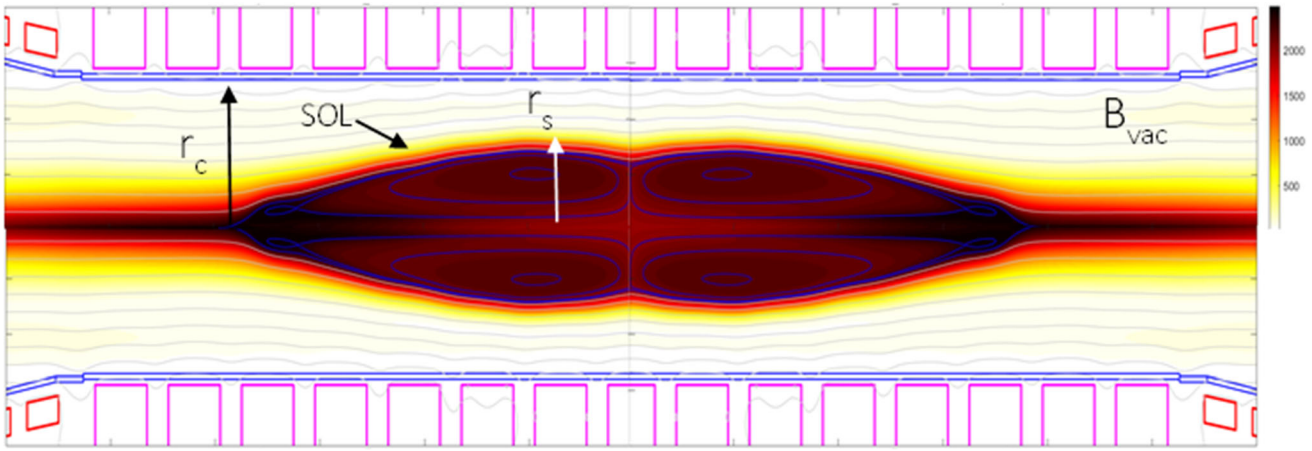

Fig. 2 2-dimensional (radial symmetry) ion temperature distribution with a merged and compressed FRC, as calculated by Cygnus [18]. The contour plot displays ion temperature in electronvolts

r_c, the external Scrape Off Layer (SOL) and the uncompressed vacuum field, B_{vac}.

In the simulations presented, results at the time of peak FRC compression and the peak fusion power output are explored. The full model includes FRC formation at low density and low temperature (less than 300 eV), acceleration and compression in a conical acceleration section, merging in a cylindrical central section, and then the rapid increase of peak magnetic field to compression. Post-merged FRCs are typically 1 keV total temperature and density 10^{21} to 10^{22} m^{-3}, depending on fill pressure. Post-merge, FRCs can retain some doublet structure, depending on their initial profiles. This behavior, while studied in depth, does not appear to have a major effect on transport [13] as long as the initial smaller radius is not significantly different than the average radius. This behavior is seen less in experimental programs, where it is believed that kinetic ion effects tend to encourage further merging. Details of the full merging and compression process, can be found in the associated references [14, 39].

Experimentally, Armstrong and Hoffman [15] measured the ion distribution in a series of careful measurements on the FRX FRC program and cold beam-driven FRC programs, [16, 17] which subsequently demonstrated similar behavior.

As will be further explained in the following section, pulsed (and steady[19]) FRCs tend to have highly disparate ion and electron temperatures. This has been shown in a number of experimental programs, including most recently, in 2021 by Helion operating at thermonuclear temperatures and measured by x-ray temperature diagnostics [1]. This phenomena is relatively straightforward; during the FRC formation and merging processes, heating is done directly to ions, either by collisional processes within the plasma during formation or by the supersonic FRC merging, in which almost all heating is directly to ions. This is also seen in the MHD figures above, particularly since the models neglect kinetic ion effects (which would tend to enhance these further). Also, as FRC plasma densities are in the range of 10^{21} to 10^{23} m^{-3}, they tend to have 1–100 ms equipartition times, which supports the maintenance of this hotter ion temperature in a pulsed system. For adiabatic compression, ions and electrons are heated proportionally, so an initial hotter ion temperature imbalance will be maintained through the entire compression cycle.

One additional physics benefit of D–He-3 systems not explored here, which would further increase the fusion power output of these systems and maintain a hotter ion temperature ratio, is that a 14.7 MeV proton in a D–He-3 plasma environment will actually impart more energy through direct nuclear elastic scattering with the fuel ions, than the traditionally modelled Coulomb collisions. This effect is well studied [20] and will both increase heating of the ions as well as increase the fusion product confinement time. In the present paper, this effect is not included, so the results are conservative. Not including this effect allows for the decoupling of the evolution of the proton production rate from transport equations.

Electron Temperature

Electron temperature uniformity is less well understood and, historically, was not expected. However, electron temperature has been widely measured in theta-pinch, rotating magnetic field, and beam-driven FRC plasmas as nearly spatially uniform. In Helion systems, from the axis to the null, the electron temperature varies within ± 15% of the average. The earliest measurements on FRX-B[21] and FRX-C[22] similarly showed this phenomenon. There are two hypotheses for this independently witnessed

behavior. First, in Helion's FRC plasmas, bulk heating is direct heating of the ions, whether from compression mechanisms or ohmic heating. Electrons typically are heated due to thermal relaxation (equipartition) with the ions, in both classical and anomalously driven heating, thus electron temperature is expected to be uniform for these systems as the ion temperature is uniform. However, for Beam-Driven FRC systems, where the primary heating is of the electrons, uniformity is also observed. The C-2 experiment, while quite cold, also showed uniform (± 20%) electron temperature profiles, [23] which were reproduced in C2-W [24]. Beyond simple heating by uniformly distributed ions, FRCs also have large parallel electron drift velocities along the magnetic field. Because the electrons are highly magnetized and can freely move along internal flux surfaces throughout the FRC both axially and between the core and radial edges, this transport results in uniform electron temperature throughout the FRC.

This is well characterized in FRC simulation and experimentation [21, 25]. In Fig. 3, a Cygnus simulation of the radial profiles of an FRC is shown with normalized ion and electron temperatures. As expected, electron temperatures near the edge and the axis are reduced as electron-thermal conduction clamps the electron temperature. Figure 4 shows a simulation for the axial and radial distribution of electron temperature.

Similar data and trends for a higher field, higher temperature FRC are shown below in Figs. 5 and 6.

Electron and Ion Density Distribution

Simple approximations for high-beta, compressed FRCs also assume constant number density with a sharp fall-off at the separatrix radius. Using these approximations, FRCs can then simply be described as a cylindrical model with a uniform-density, uniform-temperature plasma. Specifically, this model uses a fixed radius at the separatrix radius and a fixed length which uses the axial location in which the separatrix radius decreases to less than 30% of the peak radius. In the following section, a cylindrical approximation and its net effect on performance will be discussed.

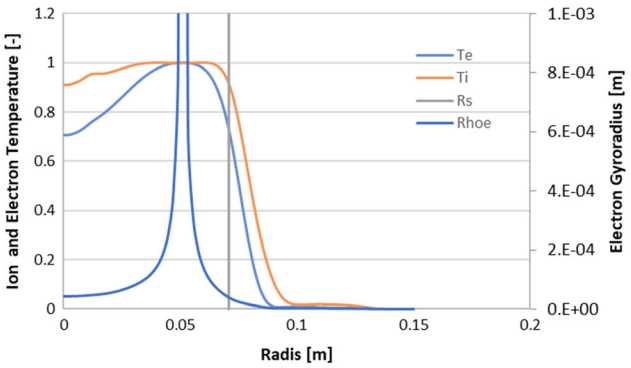

Fig. 3 Radial temperature profiles for ion and electron temperature. Note that ρ_e is the electron gyro radius

Firstly, assuming a fixed $\omega_e - \omega_i$, constant temperature, and $j_\theta = -n_e \omega_e e r$, a simple approximation for the internal magnetic field and particle density can be determined [26] by the rigid rotor profile (RR), where the local density and magnetic field are scaled to the maximum density, $n_m = p_m/(kT_{tot})$, external field, B_e, and radius, r. These approximations allow the density and magnetic field to be expressed as

$$n_e = n_m sech^2 K_{RR} u \tag{2}$$

$$B_z = B_e tanh^2 K_{RR} u \tag{3}$$

where K_{RR} is the rigid rotor profile factor (for $K_{RR} \approx 1$), and

$$u = \left({}^{r}/_{R}\right)^2 - 1 \tag{4}$$

and average beta is

$$\beta_{RR} = \frac{\int_0^{r_s} 2\pi r p dr}{2\pi R^2 p_m} = \frac{\int_0^1 p du}{2p_m} = \frac{\tanh K_{RR}}{K_{RR}} \tag{5}$$

Note, this is the average beta of the entire plasma [27]. Sample FRC internal profiles are shown in Fig. 7.

As will be shown, in practice, the rigid rotor profile is an accurate depiction of the interior of an FRC. However, the edge profile, outside the separatrix, requires further discussion. Particularly in compressed, high-temperature FRCs, the parallel thermal and particle conduction is extremely high, depopulating the effective edge and thus radial energy and particle conduction (or diffusion). Therefore, there tends to be very little plasma remaining outside of the FRC profile, leading to a sharp boundary. Three boundary profile descriptions will now be summarized.

The very sharp boundary (VSB) assumes that there is zero plasma outside of the separatrix. The modified sharp boundary (MSB), as derived from Steinhauer, [29] assumes an edge profile thickness of 1–3 ion gyro radii. The rigid rotor profile assumes $\omega_e - \omega_i$ and no enhanced transport. There are many other profile approximations developed within the community, such as the LANL diffuse profile[30], that are less appropriate for Helion's plasmas.

In practice, the edge profiles for the full simulations and the limited observations that can be done experimentally align for the internal profile and follow the rigid rotor approximation well, with an edge density profile that is sharper than the Steinhauer MSB. Figures 8 and 9 show two FRC radial profiles with a comparison between the full MHD fluid calculation, CYGNUS, the full rigid rotor approximation, and two abbreviated edge profiles. Some

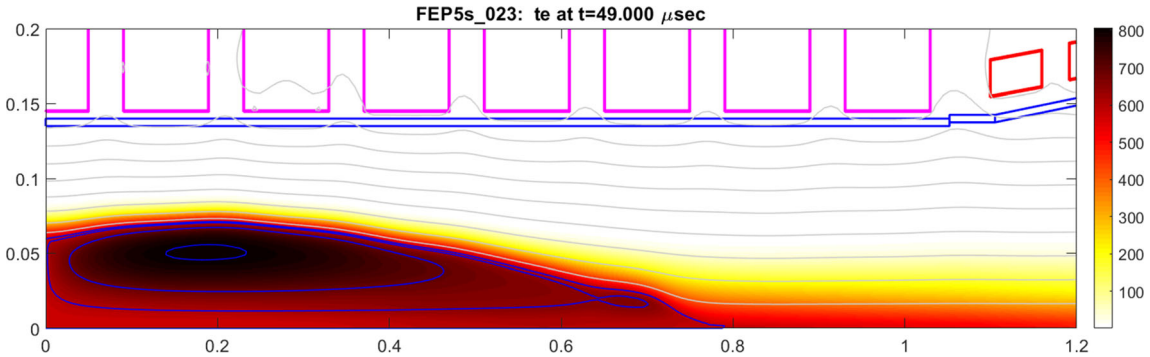

Fig. 4 2-dimensional electron temperature distribution with a merged and compressed FRC, as calculated by Cygnus. The heat map displays units of temperature (eV)

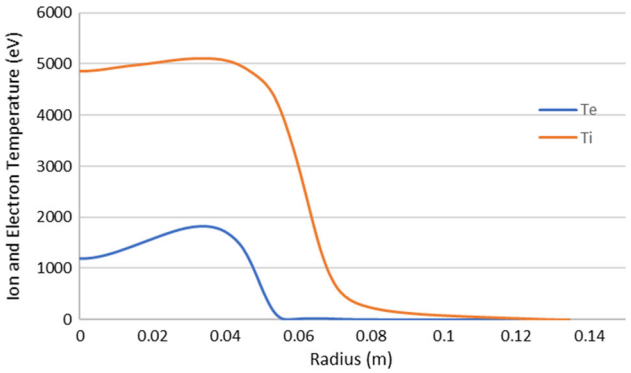

Fig. 5 Radial profiles for ion and electron temperature

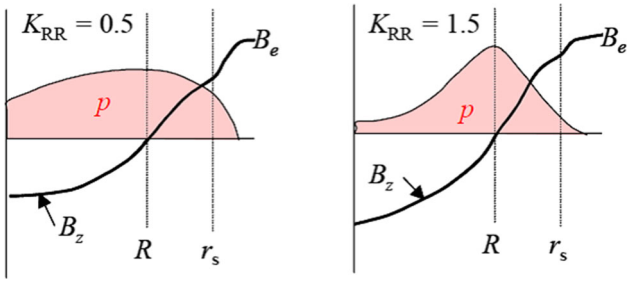

Fig. 7 Sample rigid rotor profiles for two extreme values of K_{RR}. Figure from Hoffman [26] and theory described in detail in Steinhauer [28]

limited experimental results on the external edge profile are also consistent, though for highly compressed FRCs the spatial resolution is challenging to resolve diagnostically. However, wholistic excluded flux measurements align closely with Cygnus and are commonly used to benchmark experimental results.

Energy, fusion power, and radiated power, can now be simply described. In practice, an effective length is assumed, which compensates for the decreased magnetic volume near the axial extents of the racetrack-shaped (versus elliptical) plasma.

Assuming an effective length and simplifying the terms, we find that internal plasma energy, fusion power, and radiated power scale as:

$$E = 2\pi \int_0^{r_c} nk(T_e + T_i) r dr \approx K_{RR} \int_0^{r_c} n(T_e + T_i) r dr \qquad (6)$$

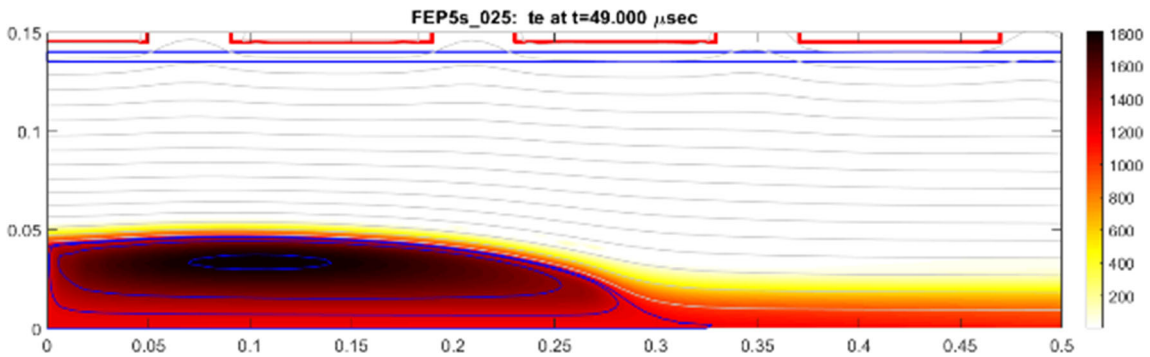

Fig. 6 2-dimensional electron temperature distribution with a merged and compressed FRC, as calculated by Cygnus. The heat map displays units of temperature

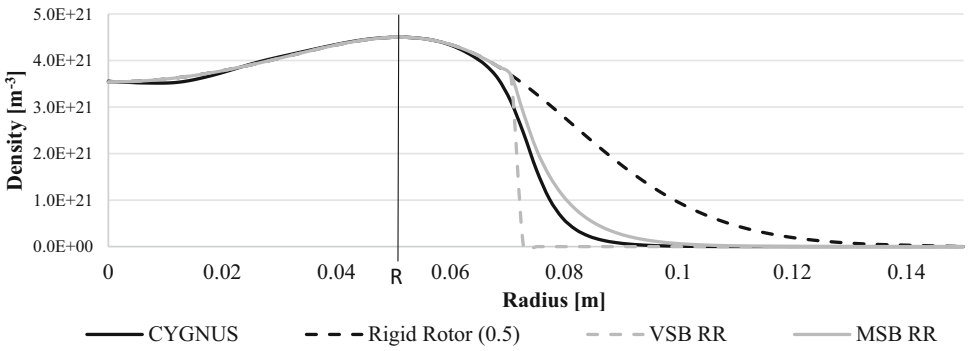

Fig. 8 FRC profiles during early compression

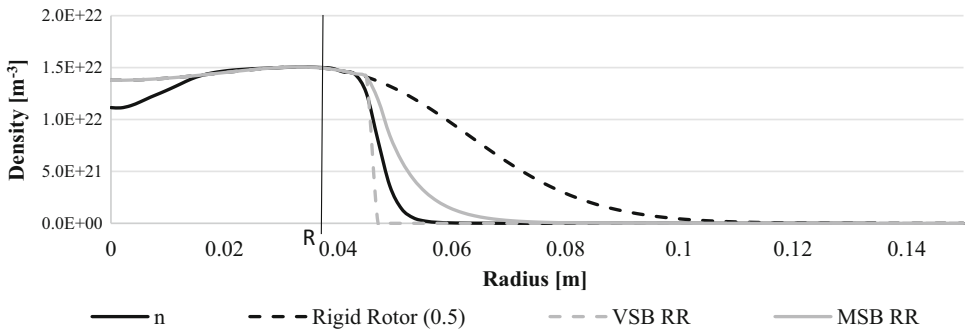

Fig. 9 FRC profiles during high compression

$$P_{fusion} = 2\pi \int_0^{r_c} n^2 \sigma v E_f r dr \approx K_{RR} \int_0^{r_c} n^2 T_i^{2.6} r dr \tag{7}$$

$$P_{Brem} = 2\pi \int_0^{r_c} \frac{Z_i^2 n_i n_e}{6 * 10^{37}} T_e^{0.5} \approx K_{RR} \int_0^{r_c} n_e^2 T_e^{0.5} r dr \tag{8}$$

where r_c is the (magnetic) coil radius. To compare the effect of a geometric approximation of constant temperature and density with the full MHD radial profiles, we can numerically integrate and normalize the result of the CYGNUS solution. Table 1 compares the three radial profiles; the full rigid rotor assumption is poor, therefore is not used in practice. The other three approximations are accurate within 11%; note that the cylindrical and RR VSB approximations underestimate fusion performance and effective energy gain. Further, the results demonstrate that less than 10% of the FRC energy, radiation losses, or fusion production is in plasma located outside of the separatrix.

Table 1 Difference in fusion-relevant scaling relations for various radial density and temperature profiles relative to Cygnus-simulated results

	n(Te + Ti)	$n^2Ti^{2.6}$	$n^2Te^{0.5}$
Cylindrical	− 8%	− 11%	− 10%
RR with VSB	− 8%	− 5%	− 4%
RR with MSB	+ 8%	+ 2%	+ 3%
RR	+ 48%	+ 23%	+ 25%

Fundamental Fusion Power Scaling with Cylindrical Profile Distributions

Helion Energy has proven the capabilities of a high-beta, pulsed magnetic fusion system operating with a deuterium and helium-3 fuel, with as much as a 10:1 ion to electron temperature ratio [1]. Unlike traditional fusion analyses, an advanced, aneutronic (disregarding side deuterium–deuterium fusion reactions) helium-3 fuel outperforms a traditional tritium fuel, primarily due to a critical missing parameter in most fusion discussions, the plasma beta. Advanced fuels such as helium-3 allow fusion systems that can utilize high-beta for efficient energy recovery to be built with an advantageous electron to ion temperature ratio due to the decreased operational density at a given output power. Further, these low—and aneutronic fuels have dramatically simpler and more cost-effective engineering and economics. The analysis below reformulates the standard fusion power equations in terms of fusion power per unit volume and radiative losses, for a fixed external magnetic field and total energy per fusion and is reported in a localized Watts per m^3 independent of specific geometry.

Fusion reaction rates are given by the density per species, n, and the Maxwellian-averaged fusion reaction

rate,$\langle\sigma v\rangle$. It is important to note that in practice the ion temperature distribution is typically not Maxwellian with an enhanced high energy tail. This results in enhanced fusion reaction rates at all temperatures and has been observed in pulsed thermonuclear fusion devices dating back to 2X [26]. Further, all pulsed FRC compression devices [40] that have reached thermonuclear conditions have observed this phenomena. Work is currently underway at Helion to theoretically model these effects. However, for this analysis, a conservative Maxwellian reaction rate will be used, with standard formulations shown in Fig. 10.

$$f = n_a n_b \sigma v \tag{9}$$

For a magnetized plasma, the average β relates the applied (external) magnetic field, B, to the average pressure,

$$k n_a T_a + n_b T_b = \beta \frac{B^2}{2\mu_0} \tag{10}$$

Assuming equal particle density and defining temperature of species 'a' as a fixed ratio of that of species 'b', h_{ab},

$$n_a = n_b = n \tag{11}$$

$$T_b = h_{ab} T_a \tag{12}$$

Thus fusion power per unit volume[31] with typical units becomes

$$P_{fusion} = \frac{\beta^2 B^4}{\left(2\mu_0 (h_{ei}+1) k T_i\right)^2} E_{fus} \sigma v \tag{13}$$

Further, assuming a Gaunt factor of 1.59, the total radiated Bremsstrahlung power (across all wavelengths) is given as a function of species ionization state, Z_i, and can be expressed in SI and resultant power units of [W/m^3] as [32]

$$P_{Brem} = \frac{Z_i^2 n_i n_e}{6 * 10^{37}} T_e^{0.5} = \frac{Z_i^2 n^2}{6 * 10^{37}} (h_{ei} T_i)^{0.5} \tag{14}$$

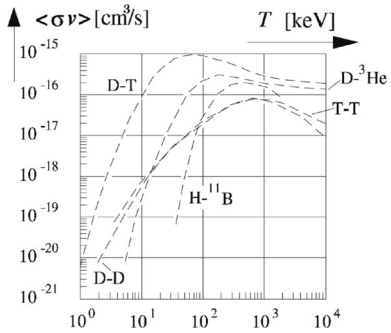

Fig. 10 Maxwellian average fusion reaction rates as a function of species

In a pulsed system (where the vacuum vessel is evacuated between pulses, and pulses are short relative to impurity-introduction timelines), Z_{eff} is very close to Zi, though, in practice, this will effectively increase radiation losses.

Cyclotron (or at several hundred keV energies and above, synchrotron) radiation can be given in SI units as a function of its transmission fraction (for a given plasma equivalent slab thickness), k_l, and the standard parameters above [33]

$$P_{cyc} = \frac{\sigma_t B^2 v_\wedge^2}{c\mu_0} \approx 6.2 * 10^{-28} k_l B_e^2 (h_{ei} T_i) n_e \tag{15}$$

Interestingly, as losses scale linearly with density and electron temperature, the power loss density is constant with temperature and fixed beta. Relativistic corrections are ignored in this analysis, as they will be small for the energies of interest. A critical requirement for cyclotron radiation is transmission and absorption, as for low electron temperatures and high electron densities radiation losses will be dominated by the absorption behavior [34]. An approximation for net transmission of synchrotron radiation is given by Rose, et al. as a function of plasma and electron frequency, ω_p and ω_{ce}, and the plasma thickness, r_s. As can be seen in SI units in the vast majority of synchrotron radiation is absorbed below 100 keV electron temperature.

$$k_l = 0.002 T_e^{7/4} r_s^{0.5} = 0.002 \frac{T_e^{7/4} (c\omega_{ce})^{0.5}}{r_s^{0.5} \omega_p} \tag{16}$$

At most temperatures the primary loss mechanism is particle and energy transport, rather than radiation, this is due to several key factors. Highly compressed FRC plasmas are unique in that there is a very sharp gradient in plasma density, as shown above. In addition, to meet key stability requirements all compressed FRCs are designed so that they are highly elongated such that purely radial transport is a good geometric approximation. During compression, FRCs will further elongate[35]. Further, the thermal conduction along field lines outside of the FRC is extremely fast such that at high temperature, there is little to no plasma outside of the separatrix. Because this area is evacuated, the parallel conduction rates has little to no effect on the cross field diffusion rates [36]. Therefore, for high temperature, highly compressed FRCs, a pure radial transport model based on Lower Hybrid Diffusion scaling is generally accepted by the FRC community [8]. The model used has been consistently validated on a range of FRC programs and is generally only deviated from when there is flux or particle addition (i.e., neutral beams) [37].

Previous FRC programs by the authors have verified these historical transport equations and added more

complex geometric terms that account for effects of end curvature [38]. Equation (17) shows the demonstrated FRC particle confinement lifetime, τ_n in units of seconds, as a function of elongation, ε, separatrix ratio, $x_s = r_s/r_c$, density, n in SI units which has been validated to over 10 keV plasma temperatures [39, 40].

$$\tau_n \approx 3 * 10^{-15} \varepsilon^{0.5} x_s^{0.8} r_s^{2.1} n^{0.6}, \tag{17}$$

FRC energy lifetimes have been found to be comparable to particle lifetime, so transport losses can be well approximated as the total particle energy and particle confinement time, particularly when radiation energy losses are accounted for separately. As FRCs have a complete vacuum boundary, thermal conduction losses are minimal. By accounting for radiation loss specifically separately, the increased losses of higher mass fuels will be more properly accounted for. This simplification is a function of FRC profile and flux[41] but for fully compressed FRCs, is generally correct. The energy transport rate for a given plasma radius [38, 39] is given by Eq. (18).

$$P_{transport} = \frac{\langle \beta \rangle \frac{B^2}{2\mu_0}}{\tau_n} \tag{18}$$

Fusion Generator Considerations

Fusion gain, Q, in a thermonuclear fusion plasma has a wide range of definitions[42], particularly for advanced fuels. For the purposes of the following discussion, Q will be represented as a conservative scientific Q_{sci}, that assumes all radiative and transport effects are energy losses and all fusion products are positive energy output. No direct energy recovery, heating power, secondary fusion production, blanket heating, or other, less-conservative metrics, are assumed for this analysis. The resultant definition in equation form is:

$$Q_{sci} = \frac{P_{fusion}}{P_{Brem} + P_{Cyc} + P_{transport}} \tag{19}$$

For a fixed magnetic field and geometric scale comparisons of the relevant fusion power output and losses due to radiation and transport in D–T systems are given in Figs. 11 and 12. This models a beam-heated (or alpha-heated) steady system in which ions and electrons are close to thermal equilibrium with electrons 50% hotter than the ions. Figure 11 shows a low-beta system (10%), while Fig. 12 shows a high-beta (100%) system. When beta is unity and field is fixed, as ion temperature is increased, density decreases. For lower temperatures the fusion reaction rate increases with temperature faster than density-squared, so net fusion power output increases. But the rate of reactions as a function of temperature slows at higher temperature, which results in decreased fusion power output. As expected, for a fixed magnetic field, a low-beta plasma with FRC transport is near or below breakeven at all temperatures. For FRC plasmas, the primary loss is particle transport, with significant radiation losses below 2 keV and above 100 keV ions. However, for a high-beta condition, D–T breakeven is possible above 3 keV, with Q_sci > > 10 and likely ignition at 10 keV. D–D fusion, even for high-beta conditions, does not break even.

Figure 13 shows the same fundamental model applied to a D–He-3 fusion system. As one would expect, a low-beta fusion plasma in D–He-3 is well below both thermal energy transport and radiation barriers. For the same input field and energy, at low beta, D–T fusion performs significantly better than any advanced fuel. D–He-3 fusion has a power density 1/20th that of D–T, a seemingly insurmountable challenge. Neither D–D, nor D–He-3[43] can exceed total radiation losses at any temperature. Further, using demonstrated FRC transport, neither D–D, nor D–He-3 fuels are net positive, and only D–T is possible in a slim operating range. However, by utilizing a high-beta configuration the picture radically evolves. In a high-beta plasma, D–He-3 can attain net positive energy. As shown in Fig. 14, by increasing for D–He-3, for a given ion temperature and assuming equilibrium ion and electrons, the fusion power output dramatically increases, and $Q_{sci} > 1$ is possible above 20 keV. This analysis assumes equilibrium ions and electrons.

Secondly, by decreasing the electron to ion temperature ratio as shown in Fig. 15 (which has been demonstrated routinely in pulsed devices [1]), the relative fusion power to Bremsstrahlung and synchrotron radiation loss ratio increases, now requiring only a minimum of 10 keV ion temperature for net gain D–He-3 operation. It is also clear that operating D–He-3 at temperatures above 40 keV now only has marginal benefits in fusion power output. Lastly, unity D–He-3 (and D–D as well) plasmas outperform a low-beta D–T plasma by over an order of magnitude in power density. One important note, in an ignited D–T (or D–He-3) plasma, particle heating primarily heats electrons (regardless of initial heating method), leading to the typically large electron to ion temperature ratios, and significantly increased radiation losses, further emphasizing the desire to remove energy directly from the fusion products prior to ignition or significant electron heating.

Commercialization

The ability to utilize a low-neutronic fuel has extensive benefits for the commercialization of fusion energy systems. Isotopic damage due to high energy neutrons and material activation drive several engineering and business decisions in fusion systems that can significantly increase cost. By utilizing a fuel that produces 2.45 MeV neutrons and several orders of magnitude less of them, less exotic

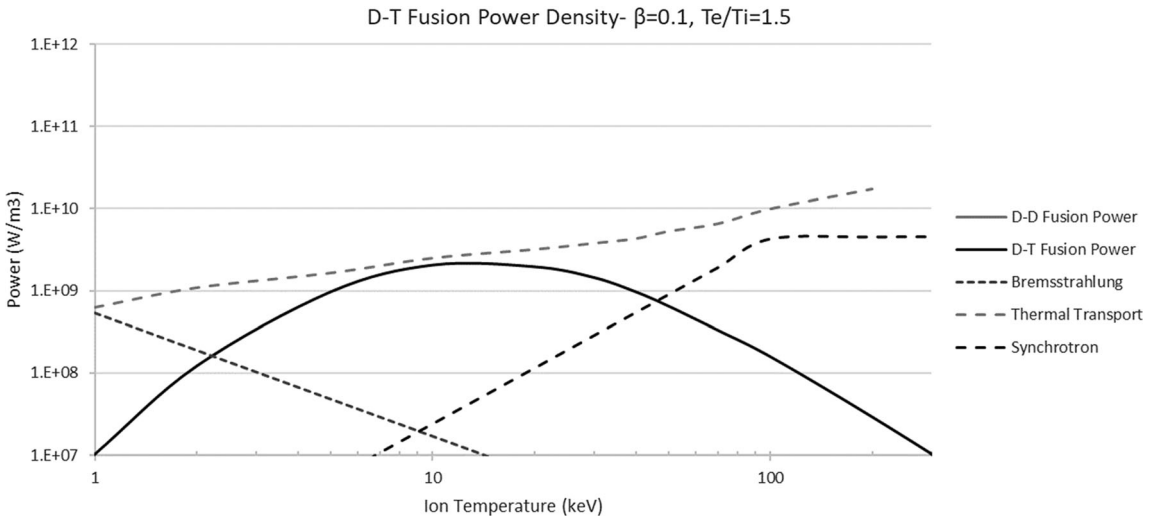

Fig. 11 Comparison of instantaneous fusion power output per unit volume for a low-beta (0.1), beam-heated D–T fusion fuel. All fusion products included (no direct recovery), all thermal, particle, radiation assumed loss

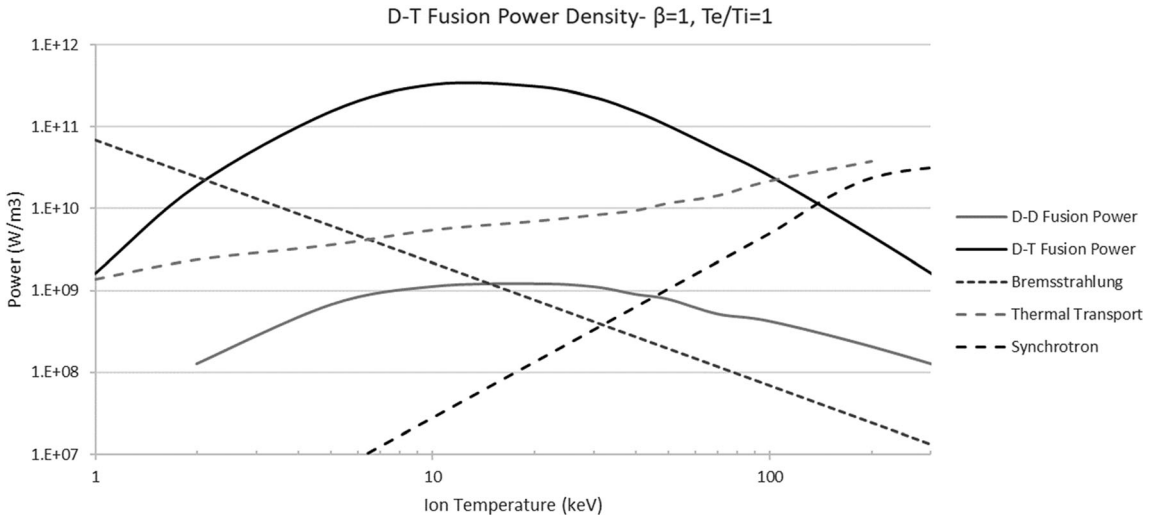

Fig. 12 Comparison of instantaneous fusion power output per unit volume for a high-beta, equilibrium, adiabatically compressed D–T fusion fuel. All fusion products included (no direct recovery), all thermal, particle, radiation assumed loss

materials may be used in a neutron environment. Further, a D–He-3 fusion system generates most of its energy with the 14.7 MeV proton and 3.6 MeV alpha particle that are produced during fusion. This enables direct energy conversion[44] which allows for the direct recovery of input magnetic energy at very high efficiencies (greater than 90%) as well as high efficiency energy extraction of charged particles. This then creates a path to commercial electricity production at lower input and output powers at smaller scale, and thus, lower capital cost. Lastly, it is believed that fusion systems that have an open topology, modular magnetic coil design, non-cryogenic magnets, and less rare materials may allow for more traditional mass production techniques for power systems, magnets, vacuum vessels, and structures. Fundamentally, these advances should allow for the production of commercial fusion systems that are lower cost than comparable low-beta approaches.

D–He-3-fueled fusion systems have several unique engineering challenges. First, and most notably, as with tritium fuel, there is little Helium-3 available terrestrially. However, unlike tritium, which requires a beryllium and lithium blanket to breed and thus requires the sourcing and permanent transmutation of other rare elements, Helium-3 can be produced from D–D fusion or the mining of extra-terrestrial sources[45]. Helion has patented a closed-cycle fusion process[46] in which the fusion reaction is operated with additional deuterium fuel, such that input deuterium is fused into He-3 and input He-3 is fused into He-4 and used to create electricity. All input and output fuel products stay

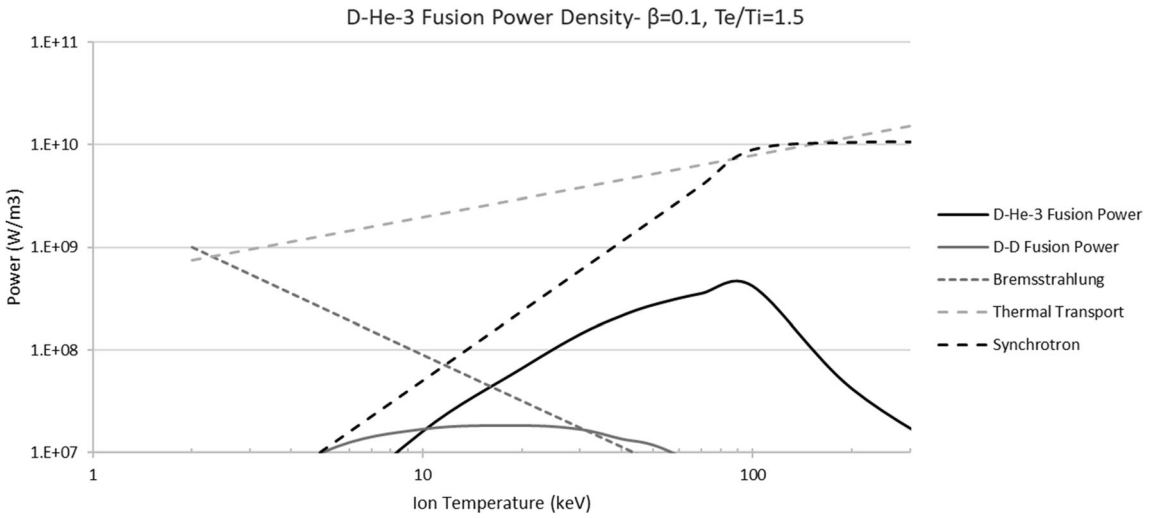

Fig. 13 Comparison of instantaneous fusion power output per unit volume for a low-beta (0.1), beam-heated D–He-3 fusion fuel. All fusion products included (no direct recovery), all thermal, particle, radiation assumed loss

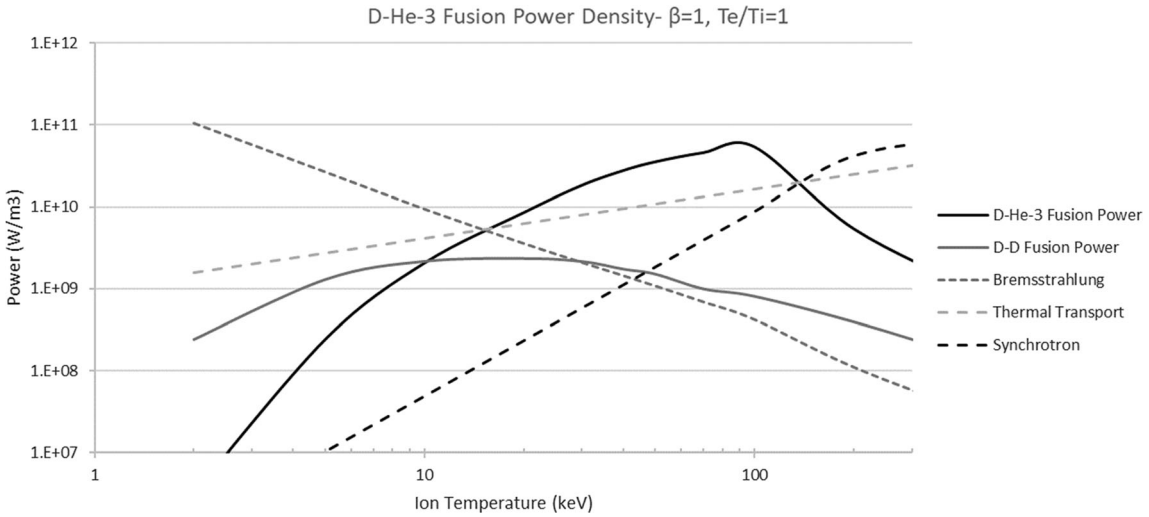

Fig. 14 Comparison of instantaneous fusion power output per unit volume for a high-beta, equilibrium, adiabatically compressed D–He-3 fusion fuel. All fusion products included (no direct recovery), all thermal, particle, radiation assumed loss

in a gaseous (or plasma) state and do not require dedicated breeding blankets nor neutron interactions. This requires a complex gas filtering system that separates the various hydrogenic and helium isotopes, which are readily commercially available. There are further business options in which a standalone D–D fusion plant generates He-3 and H-3 (which decays into He-3) and runs at a slight negative power deficit. The key to this approach is high-efficiency energy recovery to limit the effective cost by reducing electricity use. As with D–T systems, there will be tritium in a D–He-3 system, created by the D–D reaction. A tritium recovery and storage system is required for a D–He-3 system as is a radioactive materials byproduct license, however, because there is no lithium processing system, the tritium can be stored in solid, non-reversible getters which dramatically lowers radioactive release risks. The primary risk of this process is when tritium is in a gaseous or oxidized states. In the fission industry and industrial facilities it is common to store kilograms of tritium in solid getters. Helion has had operational radioactive air emission, radioactive materials, and particle accelerator shielding licenses with the Washington Department of Health for several operational fusion machines.

Status of Development Programs

Helion Energy has developed six fusion systems [1, 12, 21, 22] that have reconfirmed empirical scaling relations to plasma temperatures greater than 1 keV. The 6th generation system, Trenta, exceeded the performance

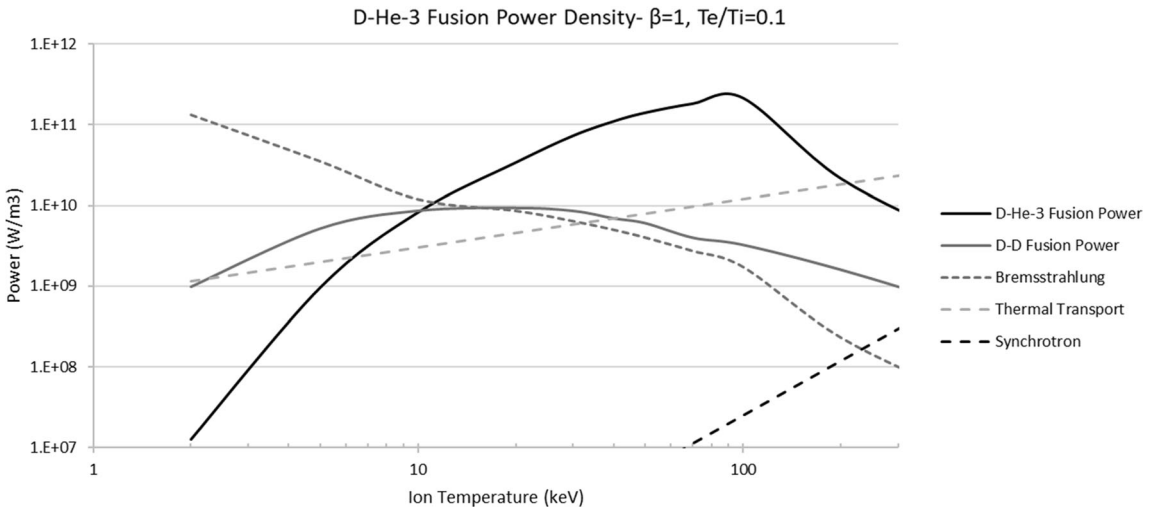

Fig. 15 Comparison of instantaneous fusion power output per unit volume for a high-beta, non-equilibrium, adiabatically compressed D–He-3 fusion fuel. All fusion products included (no direct recovery), all thermal, particle, radiation assumed loss

of previous fusion devices, creating FRC plasmas in a system with greater than 0.5 m radius, compressing to over 8 T as measured externally, and heating fusion ions over 8 keV [1] at peak compression. Industry-standard magnetic flux and field diagnostics were used to determine FRC profile and internal pressure at 100 + axial locations, Beryllium-foil x-ray diagnostics were used to diagnose electron temperature, multi-channel fiber interferometers were used to measure electron density, and a range of x-ray and optical spectroscopic and bolometer measurements were used to diagnose Bremsstrahlung and radiated power emission. Further peer-reviewed works on these diagnostic measurements on Trenta are underway as of the publishing of this manuscript. Helion is currently building its 7th generation system, Polaris, which will form FRC plasmas in excess of 1 m diameter and compress them to high field, greater than 15 Tesla. If successful, the Polaris system should generate electricity for the first time in any FRC fusion system. It is expected that Polaris will begin operation in 2024.

Conclusion

FRC plasmas typically assume constant plasma temperature within the magnetic boundary. As has been shown, due to the unique field structure of the FRC, this is both theoretically expected and observed in computational codes as well as all carefully conducted experimental programs. Further, the edge profile and vacuum insulation of an FRC is very sharp, typically a gyro orbit or less and can be approximated by several theoretical and empirical approximations. As shown, in a compressed high-beta fusion plasma, the density and temperatures can also be accurately approximated as uniform, resulting in relevant fusion metrics conservatively within 11% of the full solution. The ability to represent the FRC as a uniform, simple plasma structure is a tremendous advantage for system design, scaling analyses, and fundamental system trades.

In the above work, a cylindrical approximation is utilized to model a compressed FRC with typical thermonuclear relations for D–D, D–T, and D–He-3 fuels for a range of ion to electron temperature ratios and average beta. When beta is unity and field is fixed, as ion temperature is increased, density decreases. For lower temperatures the fusion reaction rate increases with temperature faster than density-squared so net fusion power output increases with increasing fuel temperature. At higher temperature, the reaction rate increase slows, therefore fusion power output decreases. As expected, for a fixed field, low-beta fusion plasma, D–T fusion fuel significantly outperforms all fusion fuels. However, as shown above, operating in a high-beta plasma configuration that has preferential ion to electron temperature ratios of a pulsed, magnetic fusion system yields a startling new result. For all operating conditions above 10 keV ion temperature, a high-beta D–He-3 fusion fuel not only is capable of producing significant net fusion energy, it also outperforms a low-beta D–T fusion fuel in terms of fusion output and fusion energy density. Further, 14.7 MeV high-energy protons can directly heat fuel ions through nuclear elastic scattering without Coulomb collisions. These things considered demonstrate that a high-beta D–He-3 fusion fuel may be the optimal fusion fuel for fusion commercialization.

Author contributions D.K wrote the majority of the manuscript, prepared the models, completed the analysis. R.M. prepared the

computational sections of the manuscript, completed model analysis, and reviewed the early drafts of the manuscript.

Declarations

Competing interests The authors declare no competing interests.

References

1. D. Kirtley, A. Hine, R. Milroy, C.Pihl, R. Ryan, A. Shimazu, G. Votroubek, Thermonuclear field reversed configuration plasmas in the trenta prototype. IEEE Symposium on Fusion Engineering. (2021)
2. D. Kirtley et al., Overview of staged magnetic compression of FRC targets. APS Division of Plasma Physics Meeting. (2018).
3. D.Kirtley, et al., Vacuum vessel and divertor design and results of 16 month operation of the Trenta Magneto-Inertial Fusion prototype. IEEE symposium on fusion engineering, 2021
4. J.F. Santarius et al., Final report for the field-reversed configuration power plant critical-issue scoping study. University of Illinois, Fusion Studies Laboratory, Urbana, IL (US); University of Wisconsin-Madison, WI; University of Washington (US) (2001)
5. J.F. Santarius et al., Could advanced fusion fuels be used with today's technology? J. Fus. Energy **17**(1), 33–40 (1998)
6. L.C. Steinhauer, T.P. Intrator, Equilibrium paradigm for field-reversed configurations and application to experiments. Phys. Plasmas **16**(7), 072501 (2009)
7. H.Y. Guo et al., Formation of a long-lived hot field reversed configuration by dynamically merging two colliding high-β compact toroids. Phys. Plasmas **18**(5), 056110 (2011)
8. A.L. Hoffman, R.D. Milroy, Particle lifetime scaling in field-reversed configurations based on lower-hybrid-drift resistivity. Phys. of Fluids **26**(11), 3170–3172 (1983)
9. L.C. Steinhauer, R.D. Milroy, J.T. Slough, A model for inferring transport rates from observed confinement times in field-reversed configurations. Phys. Fluids **28**(3), 888–897 (1985)
10. Y. Wang, R. Kulsrud, H. Ji, An analytic study of the perpendicularly propagating electromagnetic drift instabilities in the magnetic reconnection experiment. Phys. Plasmas **15**(12), 122105 (2008)
11. L. Steinhauer, D.C. Barnes, Tearing relaxation and the globalization of transport in field-reversed configurations. Phys. Plasmas **16**(9), 092505 (2009)
12. MITRE. Prospects for low cost fusion development. Report on behalf of JASON. JSR-10-011 (2018). https://irp.fas.org/agency/dod/jason/fusiondev.pdf
13. R.D. Milroy, J.U. Brackbill, Toroidal magnetic field generation during compact toroid formation in a field-reversed theta pinch and a conical theta pinch. Phys. Fluids **29**(4), 1184–1195 (1986)
14. G. Votroubek et al., Compression of dynamically formed and merged FRCs. APS Division of Plasma Physics Meeting Abstracts. 49. (2007)
15. W.T. Armstrong et al., Field-reversed experiments (FRX) on compact toroids. Phys. Fluids **24**(11), 2068–2089 (1981)
16. D. Gupta, et al. Time-evolution of ion-temperature radial profiles for high performance FRC (HPF) plasma in C-2. APS Division of Plasma Physics Meeting Abstracts. 2014. (2014)
17. Nations, M., et al., Measurements of impurity ion temperature and velocity distributions via active charge-exchange recombination spectroscopy in C-2W. Rev. Sci. Instrum. **92**(5), 053512 (2021)
18. A. Shimazu, D. Barnes et al. Cygnus code simulation of magnetoshell aerocapture and entry system. APS Division of Plasma Physics. (2017)
19. R. Milroy, C. Kim, and A. Necas, NIMROD simulations of the stabilization of the FRC tilt instability with energetic ion beams. APS Division of Plasma Physics Meeting Abstracts. 54. (2012)
20. Y. Nakao et al., Time dependent multigroup analysis of nuclear elastic scattering effects in advanced fuel fusion plasmas. Nucl. Fus. **28**(6), 1029 (1988)
21. W.T. Armstrong, R.K. Linford, J. Lipson, D.A. Platts, E.G. Sherwood, Field-reversed experiments (FRX) on compact toroids. Phys Fluids **24**(11), 2068–2089 (1981)
22. D.J. Rej, W.T. Armstrong, Electron temperature measurements in the field-reversed configuration experiment FRX-C. Nucl. Fus. **24**(2), 177 (1984)
23. B.H. Deng, J.S. Kinley, J. Schroeder, Electron density and temperature profile diagnostics for C-2 field reversed configuration plasmas. Rev. Sci. Instrum. **83**(10), 10E339 (2012)
24. H. Gota et al., Formation of hot, stable, long-lived field-reversed configuration plasmas on the C-2W device. Nucl. Fus. **59**(11), 112009 (2019)
25. T. Roche et al., Edge/SOL plasma parameter/magnetic field profile and fluctuation measurements at C-2U mid-plane. APS Division of Plasma Physics Meeting Abstracts. 2016. (2016)
26. A. Hoffman, Field reversed configurations. University of Washington Text Book. (2006)
27. T.K. Fowler, Mirror theory, in *Fusion, part B*. ed. by E. Teller (Elsevier, Hoboken, 1981), p.350
28. L.C. Steinhauer, Review of field-reversed configurations. Phys. Plasmas **18**(7), 070501 (2011)
29. L.C. Steinhauer, H.L. Berk et al., Coupled transport in field-reversed configurations. Phys. Plasmas **25**(2), 022503 (2018)
30. R.L. Spencer, M. Tuszewski, R.K. Linford, Adiabatic compression of elongated field-reversed configurations. Phys Fluids **26**(6), 1564–1568 (1983)
31. G.V. Oost, R. Eckhard, Thermonuclear burn criteria. Fus. Sci. Technol. **53**(2), 16–26 (2008)
32. A. Richardson, *2019 NRL plasma formulary* (US Naval Research Laboratory, Washington, DC, 2019)
33. J.M. Dawson, Advanced fusion reactors, in *Fusion, part B*. ed. by E. Teller (Academic Press, London, 1983), p.465
34. D.J. Rose, *Feasibility of power by nuclear fusion* (Oak Ridge National Lab, Tenn, 1968)
35. T.P. Intrator, R.E. Siemon, P.E. Sieck, Adiabatic model and design of a translating field reversed configuration. Phys. Plasmas **15**(4), 042505 (2008)
36. L.C. Steinhauer, Electron thermal confinement in the edge plasma of a field-reversed configuration. Phys. Fluids B **4**(12), 4012–4018 (1992)

37. M. Inomoto, T. Asai, S. Okada, Neutral beam injection heating on field-reversed configuration plasma decompressed through axial translation. Nucl. Fus. **48**(3), 035013 (2008)
38. L.C. Steinhauer, Improved analytic equilibrium for a field-reversed configuration. Phys. Fluids B **2**(12), 3081–3085 (1990)
39. G. Votroubek et al., Formation of a stable field reversed configuration through merging. J. Fus. Energy **27**(1), 123–127 (2008)
40. J. Slough, G. Votroubek, C. Pihl, Creation of a high-temperature plasma through merging and compression of supersonic field reversed configuration plasmoids. Nucl. Fus. **51**(5), 053008 (2011)
41. M. Tuszewski, Field reversed configurations. Nucl. Fus. **28**(11), 2033 (1988)
42. S. Wurzel, S. Hsu, Progress toward fusion energy breakeven and gain as measured against the Lawson criterion. Phys. Plasmas **29**(6), 062103 (2022)
43. T.K. Fowler, Mirror theory, in *Fusion, part B*. ed. by E. Teller (Elsevier, Hoboken, 1981), p.353
44. T.A. Oliphant, F.L. Ribe, T.A. Coultas, Direct conversion of thermonuclear plasma energy by high magnetic compression and expansion. Nucl. Fus. **13**(4), 529 (1973)
45. J.F. Santarius, Lunar 3He and fusion power lunar 3He and fusion power. Fus. Technol. **325**, 350 (2004)
46. J.T. Slough, D.E. Kirtley, C.J. Pihl (2022) Advanced fuel cycle and fusion reactors utilizing the same. US Patent No. 11,469,003. 11 Oct. 2022